ADVANCED FUNCTIONAL MATERIALS
www.afm-journal.de

www.MaterialsViews.com

# In-Plane Self-Turning and Twin Dynamics Renders Large Stretchability to Mono-Like Zigzag Silicon Nanowire Springs

*Zhaoguo Xue, Mingkun Xu, Xing Li, Jimmy Wang, Xiaofan Jiang, Xianlong Wei, Linwei Yu,* Qing Chen,* Junzhuan Wang, Jun Xu, Yi Shi, Kunji Chen, and Pere Roca i Cabarrocas*

**Crystalline Si nanowire (SiNW) springs, produced via a low temperature (<350 °C) thin film technology, are ideal building blocks for stretchable electronics. Herein, a novel cyclic crystallographic-index-lowering self-turning and twin dynamics is reported, during a tin-catalyzed in-plane growth of SiNWs, which results in a periodic zigzag SiNW without any external parametric intervention. More interestingly, a unique twin-reflected interlaced crystal-domain structure has been identified for the first time, while in situ and real-time scanning electron microscopy observations reveal a new twin-triggering growth mechanism that is the key to reset a complete zigzag growth cycle. Direct "stress–strain" testing of the SiNW springs demonstrates a large stretchability of 12% under tensile loading, indicating a whole new strategy and capability to engineer mono-like SiNW channels for high performance stretchable electronics.**

## 1. Introduction

Crystalline silicon (c-Si) has been well known as a "rigid" and "brittle" material that allows little stretchability. When produced in a form of quasi-1D silicon nanowires (SiNWs), c-Si becomes largely bendable,[1–3] but still hardly stretchable as irreversible plastic deformation or breakage will develop under tensile strain up to only 3% (and even less for thicker nanowires with diameter >60 nm, where their Young's modulus resumes to the bulk value).[4] An elegant strategy to impart extra stretchability to the rigid SiNWs is to engineer them into an "elastic" form, for instance a 2D spring[5] or even 3D nanocoil.[6,7] Though helical $SiO_2$ or $SiO_x$ nanocoils have been produced via iron-catalyzed vapor–liquid–solid (VLS) growth,[6,7] the growth temperature is extremely high (>1160 °C) and the silica nanocoils are by themselves basically insulating dielectric. So, if the crystalline Si NWs can be grown directly into elastic nanosprings at low temperature (<350 °C), a wide spectrum of potentially far-reaching applications could be envisioned, which may include, for example, high mobility wearable electronics,[5,8,9] bio or mechanical sensors,[10,11] and skin prosthesis with highly localized mechanical and thermal perception.[12,13]

An increasing effort has been devoted to this end in recent years, for example, (i) curly SiNWs are elaborated by mechanical buckling of initially straight SiNWs with the aid of polymer substrate contraction;[8] (ii) kinked vertical NWs are produced by periodic changes of the chamber pressure[14,15] or chemical vapor;[16] and (iii) electron beam lithography patterning has also been used to define nanoscale channels to force VLS-grown SiNWs grow into wavy shapes.[17] However, none of these approaches has been able to demonstrate a single-run fabrication without any external intervention, or has to resort to post-growth manipulation that could inflict structural damage to the nanowires. Meanwhile, in view of device fabrication, SiNWs lying on a substrate are far easier to handle and process. It is thus preferable to accomplish such a high level of morphology engineering of SiNW springs directly in-plane (or on-plane) via a single self-assembly growth, which is practically important for prototyping or assembling stretchable macroelectronics in large scale.

In parallel, it is well known that the emerging of twin planes has been a common cause of growth direction change during the growth of both silicon[16] and III-V group[18] nanowires, which if appearing in a controllable manner will provide a straightforward way to engineer the morphology of SiNWs.[19]

Z. Xue, M. Xu, J. Wang, X. Jiang, Prof. L. Yu, J. Wang, Prof. J. Xu, Prof. Y. Shi, Prof. K. Chen
National Laboratory of Solid State Microstructures/School of Electronics Science and Engineering/Collaborative Innovation Center of Advanced Microstructures
Nanjing University
210093 Nanjing, P. R. China
E-mail: yulinwei@nju.edu.cn; linwei.yu@polytechnique.edu
X. Li, Prof. X. Wei, Prof. Q. Chen
Key Laboratory for the Physics and Chemistry of Nanodevices
Peking University
100871, Beijing, P. R. China
E-mail: qingchen@pku.edu.cn
Prof. L. Yu, Prof. P. Roca i Cabarrocas
LPICM, CNRS
Ecole Polytechnique
Université Paris-Saclay
91128 Palaiseau, France

**DOI: 10.1002/adfm.201600780**

However, whether this unique self-automated twinning dynamics can be mastered in a deterministic way has not yet been well fully explored. If successful, this capability will be both fundamentally important and practically useful.

In this work, we demonstrate for the first time a novel cyclic crystallographic-index-lowering self-turning and twin dynamics, during a tin-catalyzed self-assembly growth of in-plane SiNWs, which has been able to produce 2D SiNW springs with a large stretchability, as witnessed in a series of "stress–strain" tests that showcase a linear response under tensile loading up to 12% (when straight SiNWs tolerate only 3%). Importantly, this has been achieved in a single-run self-assembly growth at a rather low growth temperature ≈350 °C, without the intervention of any external control. A crystallographic orientation-dependent growth balance model has been proposed to account for this unique automated wavy growth dynamics.

## 2. Results and Discussion

The fabrication procedure of the in-plane SiNWs, via an in-plane solid–liquid–solid self-assembly growth mechanism,[20–22] has been illustrated schematically in **Figure 1**a–c, which involves mainly (i) a tin (Sn) droplet formation, (ii) an a-Si:H coating as feeding thin film precursor, and (iii) a final annealing (see the Experimental Section for more details). The driving force for the lateral growth is assigned to the different Gibbs energy of Si atoms experienced in an amorphous or crystalline phase, $\Delta G \approx 0.1$ to 0.15 eV.[23,24] During the in-plane SiNW growth, as depicted in **Figure 2**a, the Sn catalyst droplet is "pulled" ahead by the front a-Si:H/Sn absorption interface (the red curve), where Si atoms are dissolved into the liquid Sn and diffuse through the catalyst droplet to deposit at the rear side (the green curve). Typical scanning electron microscopy (SEM) images of the as-grown SiNW springs are shown in Figure 1d–f, where the in-plane SiNW springs grow into the "open" area (covered by a-Si:H) with an initial diameter of ≈200 nm and a length of tens of micrometers. The regions appearing white on both sides of the in-plane SiNWs are empty of a-Si:H, left by a wider absorption swath of the leading Sn catalyst droplet. The Sn catalyst droplets are ≈500 nm in diameter, but shrink slowly to the end of the in-plane SiNWs, as seen in Figure 1d,f, and eventually split into a myriad of tiny tails that merge into the surrounding a-Si:H matrix. Selective etching of the remnant a-Si:H layer by a $H_2$ plasma at 120 °C reveals the spreading tails of tiny branches (<10 nm wide) as seen in the enlarged SEM inset of Figure 1d. Scrutinizing the a-Si:H edges in the inset of Figure 1e discloses bright Sn spots decorated along the trench edges, which accounts partially for the constant loss of Sn during the in-plane growth.

It is important to note that the zigzag growth of SiNWs is highly reproducible with the choice of Sn as a new catalyst material, which is an important guarantee for setting up a comprehensive investigation of the growth dynamics and testing the mechanical properties of the zigzag SiNW springs. Compared to other metal catalysts such as indium and gallium,[20] Sn has a much higher solubility of Si and thus in principle provides a larger driving force for the lateral growth and also a stronger interface interaction required to trigger a regular zigzag growth dynamics. For a given a-Si:H thin film of 20 nm, only the Sn droplets with a diameter of 200–500 nm will successfully kick off. Smaller or larger catalyst droplets either diminish quickly into flat tail-like structures or suffer from an insufficient Si supply to activate the lateral growth, respectively.

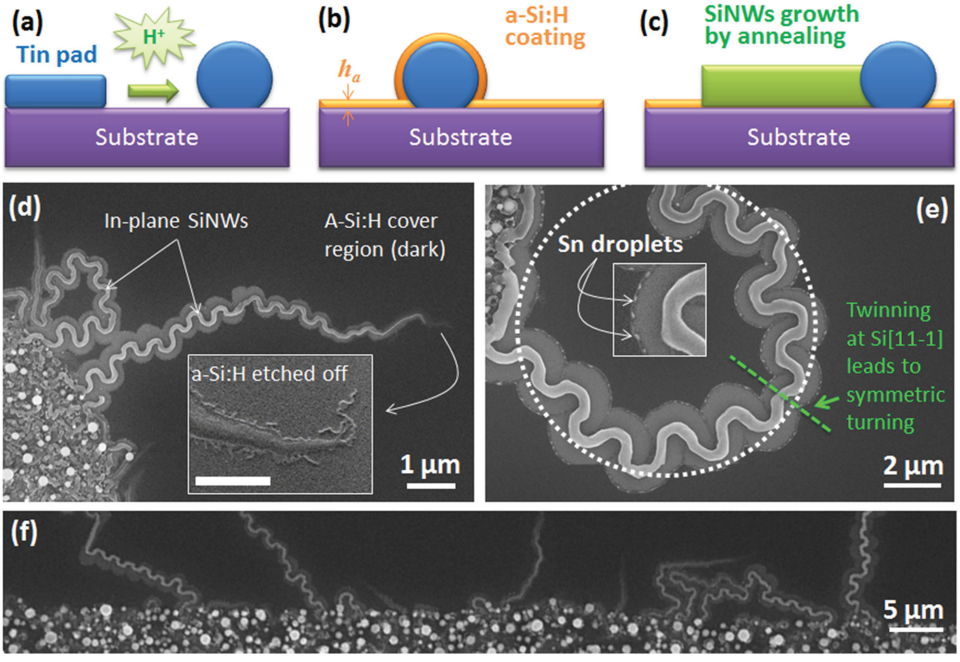


**Figure 1.** Fabrication procedure and SEM images of the zigzag SiNWs: (a)–(c) illustrate the key fabrication steps of a Sn-catalyzed in-plane growth of SiNWs; (d)–(f) showcase the typical SEM images of the zigzag SiNWs, with an enlarged view of the final end of the in-plane SiNW presented in the inset of (d), where the remnant a-Si:H layer has been selectively etched off.

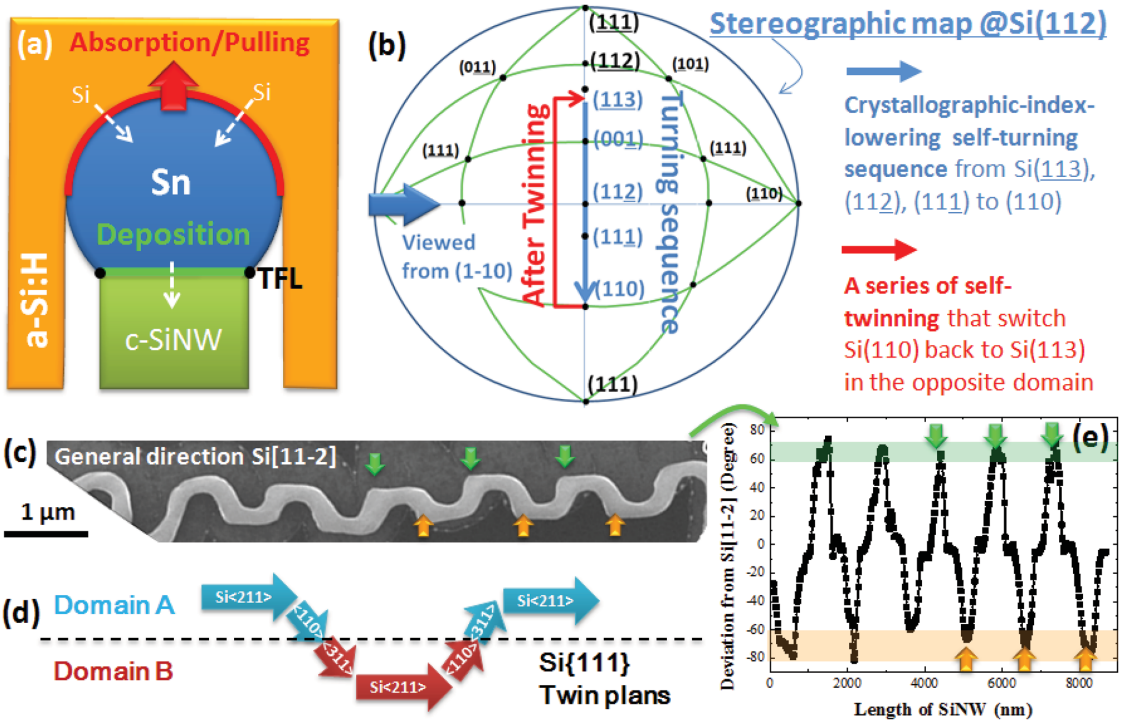


**Figure 2.** Illustrations for the growth configuration and mechanism of the in-plane SiNWs: (a) depicts the front absorption and the rear deposition interfaces, as well as the triple-phase-lines (TFL) marked by two black spots; (b) illustrates the in-plane turning-twinning sequence in a Si[11-2]-centered stereographic projection mapping; (c) shows a close SEM view of a zigzag SiNW segment, with the extracted growth direction deviation (away from the general Si<211> direction) being plotted in (e) as a function of the length of SiNW; (d) illustrates the orientation switching sequence during a complete zigzag turning-twinning circle, where the twin planes delimitate the boundaries between two interlaced crystal domains of A or B.

This leads to an effective "self-selection" of the SiNWs pulling-out from the Sn pad edge, and all of them having similar initial diameters, proportional to the catalyst diameter. Meanwhile, it is also important to note that, according to experimental observations, the diameter of the in-plane zigzag SiNWs is basically proportional to the size of the catalyst droplets, and thus thinner SiNWs can be produced with smaller Sn droplets given a "matched" a-Si:H layer thickness to guarantee a balanced in-plane growth.

A close scrutiny of the regular SiNW spring in Figure 2c shows that the "zigzag" growth involves a sequence of regular orientation switching, plotted in Figure 2e, in terms of the deviation angle from the main advancing direction (along Si[11-2]) against the length of SiNW. In **Figure 3**, we present a high resolution transmission electron microscopy (HR-TEM) characterization of such a zigzag SiNW transferred onto a copper grid. As we can see, a regular and periodic self-turning dynamics has been superimposed upon an in-plane growth, in general, along the Si[11-2] direction. Remarkably, there are at least four clearly resolved turnings in each complete cycle, which is in strong contrast to those relatively simple kinking geometries observed in the VLS nanowires with usually only a single type of turning angle.[14,15,18,19] This indicates a very different mechanism for this in-plane SiNW spring structure, other than a simple twin-kinking dynamics. Meanwhile, we note that a multistep or continuous turning can better accommodate and dissipate the large stress and strain and thus serve as a far more "resilient" spring structure than simple zigzag.[14,15,18,19]

Zooming into the structural details of the SiNW spring reveals interesting interlaced crystal domain structures, as presented in the HR-TEM images in Figure 3, with monocrystal segments/or domains delimitated by a series of parallel twin planes located at the middle of the turning arms as highlighted by the white-dashed lines. For the convenience of discussion, the segments lying to the left or to the right of the twin planes are labeled as Domain A (in red) or Domain B (in green) in Figure 3, respectively. Surprisingly, despite being separated far from each other, the segments in the same Domain group are found to be in a "coherent" lattice, as inferred from their identical 2D Fourier transform patterns taken in the separated Domains with the same labels of A or B. This interlaced twin-separated domain structure, with such a precision and ordering, has never been documented so far.

More strikingly, we found that the self-turning sequence taking place within each Domain follows a crystallographic-index-lowering order, as summarized in Figure 2b. Taking the turning sequence in Domain A as an example, apart from the last twin plane, the SiNW will first grow along the Si[113] orientation, then followed by a turning to the right into Si[11-2], and after a while into Si[110], as witnessed in Figure 3 and summarized and illustrated in Figure 2d. A more straightforward viewpoint of this feature can be obtained by drawing a trace-line of all these directions in a Si[11-2]-centered stereographic projection mapping, as seen in Figure 2b. At the end of the index-lowering turning sequence in one Domain, a set of Si[111] twin plane will happen in the midway of the

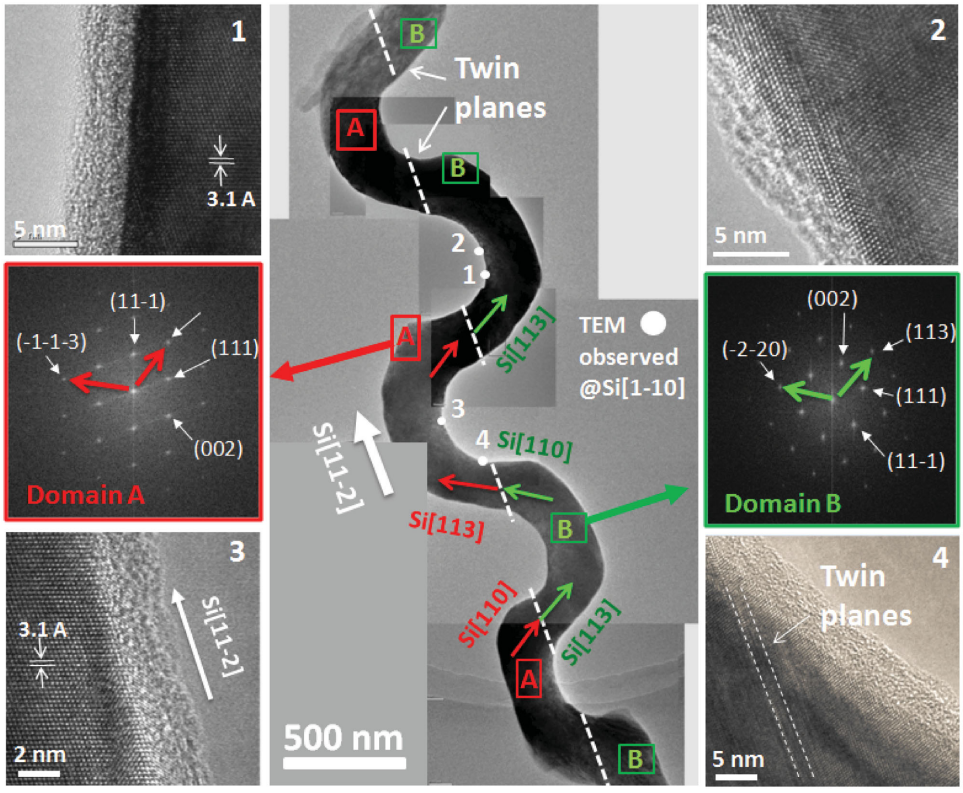


**Figure 3.** HR-TEM characterizations of a segment of a zigzag SiNW. The central image shows the reconstruction of the whole SiNW by adding up local HR-TEM images, with a series of parallel white dash-lines marking the locations of twin planes, and green or red arrows indicating the local growth orientation in Domain A or B; Fourier transform diffraction patterns are taken at different segments in Domain A or Domain B; The lattice images of the SiNW segments are sampled at 4 different places, as marked by the white-out labels from 1 to 4 in the central image, and shown in more details in the 4 corresponding corner panels.

turning arm. As seen in Figure 3 and schematically depicted in Figure 2d, after these twin planes, the local relatively low-index orientation of Si[110] in Domain A is aligned into a high-index orientation of Si[113] in Domain B. In other words, this twins "reset" the turning sequence back into a high-index one, thus allowing a new turning sequence to proceed in a twin-reflected Domain, while in general the zigzag SiNW can advance still along the Si[11-2] direction. Interestingly, this self-developed midway twinning has come to existence without the need of any external parameter adjustment (for example by modulating the growth temperature of the precursor pressure as reported in refs. [18] and [19]). In addition, while this turning-twinning sequence can be rather constant, other twin planes could also be introduced at the Si(11-1) plane (see the transient direction point after Si(11-2) in the trace-line in Figure 2c), but only occasionally and in a much less frequency under current growth conditions. Once happened, a symmetric folding of the overall zigzag SiNW structure at the Si(11-1) plane leads to a larger zigzag circle as seen for instance in Figure 1e. Meanwhile, all these growth directions involved in the turning-twin sequence are co-planar vectors, being normal to the observing direction of Si[1-10], an interesting natural constraint imposed by the in-plane SiNW growth.

Further on, in situ "real-time" SEM observations of the zigzag SiNW growth help to identify critical aspects of this peculiar self-twinning dynamics, thanks to the fact that the in-plane growth does not require gaseous supply, that otherwise would degrade the high vacuum environment in SEM. **Figure 4** presents six snapshots of the Sn-catalyzed SiNW growth. As we can see, the width of the front a-Si:H/Sn absorption interface ($W_{abs}$, marked by a red curve) is always wider than that of the rear Sn/SiNW deposition interface ($W_{nw}$, by the green line) with a basically constant ratio of $\alpha \equiv \frac{W_{nw}}{W_{abs}} \approx 0.4$ to 0.5. This ratio can also be inferred from the diameter distribution histograms of the activated zigzag SiNW growth presented in **Figure 5**a. Another finding is that, in order to maintain a balanced in-plane growth, the absorption cross section area ($\approx W_{abs} h_a$) is always proportional to the deposition cross-section of the zigzag SiNWs ($\approx W^2_{nw}$), as witnessed in the statistic plots and the linear fitting presented in Figure 5b.

As seen in Figure 4b or c, the turning direction of the catalyst/SiNW, at $t = 47$ s (or $t = 120$ s), is always to the left or the right side with a shorter sideline. According to the HR-TEM characterization in Figure 3, the continuous turning dynamics, in a crystallographic-index-lowering sequence (energetically favorable), will not trigger any twin formation and thus leaving a high quality mono-like Si lattice in the domains. Rather, when the growth proceeds to a critical point, where the catalyst droplet touches the empty trench region (without a-Si:H coating supply) produced by itself in the last cycle, as seen in Figure 4d at $t = 198$ s, the turning direction is forced to reverse.

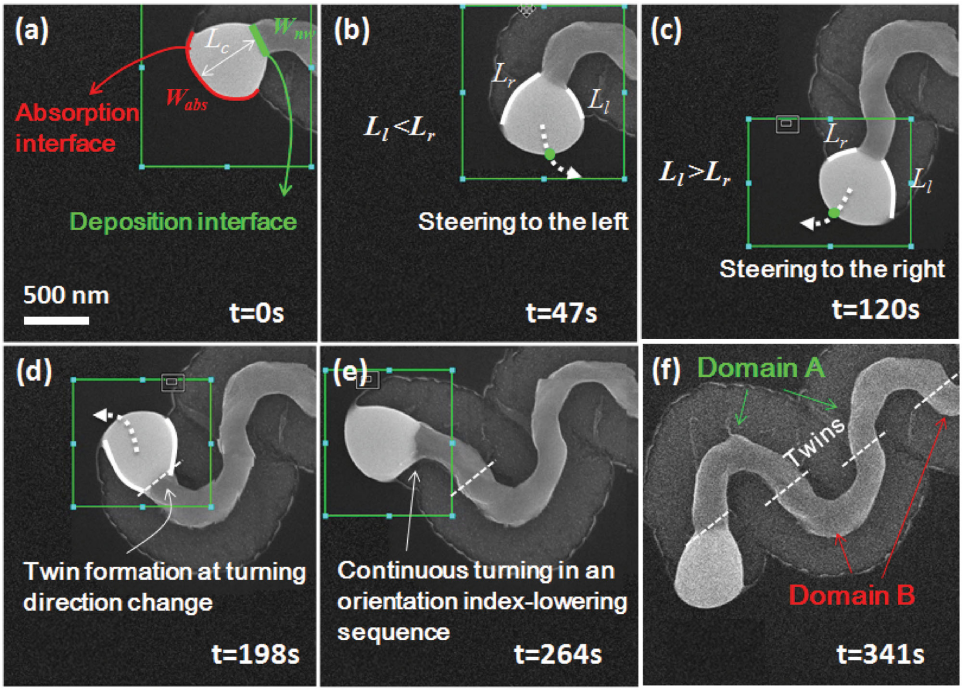


**Figure 4.** In situ SEM observation of an in-plane zigzag growth of SiNWs led by a Sn catalyst droplet. (a)–(f) show the real-time SEM imaging taken in a series of time steps at $t$ = 0, 47, 120, 198, 264, and 341 s, respectively.

At this moment, the rear deposition interface just rests at the midway of the turning arm, exactly the same place where parallel twin planes are observed in the HR-TEM characterizations in Figure 3. This seems to indicate a direct link between the twin plane formation and the change of turning direction during the in-plane SiNW growth, and this novel self-automated twin-triggering mechanism is also fundamentally different to those behind the kinking phenomena observed in the gas-feeding VLS growth of SiNWs.[14–16,18,19]

It is also noteworthy that, compared to the top-down fabrication, a self-automated bottom-up growth of regular zigzag Si nanowire springs represents a rather simple, low cost, and low temperature nanostructuring method that requires neither high resolution lithography nor multisteps processing. Importantly, this self-assembly growth leads to a high crystal quality and naturally strain-relaxed turnings without any pattern-etching or buckling damages. Nevertheless, compared to the top-down zigzag patterning, the self-assembly zigzag growth falls short of precise location and dimension control. To counter these drawbacks, a viable strategy will rely on a fine-tuning of the plasma treatment that can help to narrow the size dispersion of initial catalyst droplets and thus the produced zigzag Si nanowires. Meanwhile, an important feature of this in-plane Si nanowire growth is that it can be easily confined or directed by prepatterned step lines, as demonstrated in our previous work on straight Si nanowires,[21] and this unique feature could also be exploited to position the in-plane zigzag growth into prescribed locations and alignment.

To develop further understanding of this self-turning and twin dynamics, we come to analyze the detailed growth balance conditions for a Sn-catalyzed in-plane SiNW growth. First of all, according to the Arrhenius plot of the zigzag growth rate in Supporting Information Figure S.1, the activation energy barrier of the Sn-catalyzed in-plane SiNW is determined to be ≈1.4 eV, which is close to the activation energy of the rate-limited "nucleation formation step" in typical VLS SiNWs growth (≈1.3 eV),[25,26] implicating that the 2D "nucleation seed" generation rate is the most probable limiting kinetic step here. Note that, the Sn-catalyzed zigzag growth can be triggered over a wide range of annealing temperatures (from 300 to 400 °C), as witnessed in the in situ SEM images shown in Supporting Information Figure S.2, but with an increased period length and larger swing amplitude.

It has been established that the triple phase lines (TFL; as two projected points marked in Figure 2a), where vacuum, liquid, and solid phases join,[27,28] are the preferential sites for nursing new stable nucleus. We thus write down the general generation rate $R_{gen}$ of new nuclei at the two TFL sites as

$$R_{gen} = f_0 e^{-\frac{G_b}{kT}} = f_0 e^{-\frac{\pi K^2}{Ln(C_{Si}/C_0)}}, \text{ with } K \equiv a^2\gamma/kT \quad (1)$$

where $a = \Omega_{Si}^{1/3}$ is the atomic dimension of Si atoms and $G_b = kTLnS^*\pi K^2$ is the nucleation energy barrier for forming a stable nucleus against being dissolved back into solution, $f_0 \approx 10^{13}$ s$^{-1}$ is the attempt frequency, and $S \equiv C_{Si}/C_0$ is the supersaturation of the dissolved Si atoms with respect to equilibrium concentration $C_0$ at the Sn/c-Si interface.

Once a new nucleation site is installed, according to a Terrace-Ledge-Kink model,[29,30] the nucleus provides favorable kink "attaching" sites to incorporate supersaturated Si atoms from the Sn catalyst droplets, with a rate of $R_{in} = B(C_{Si} - C_0)$, where $B$ is a prefactor independent of $C_{Si}$. Then, these 2D nucleus kink sites/or lines annihilate upon the completion of

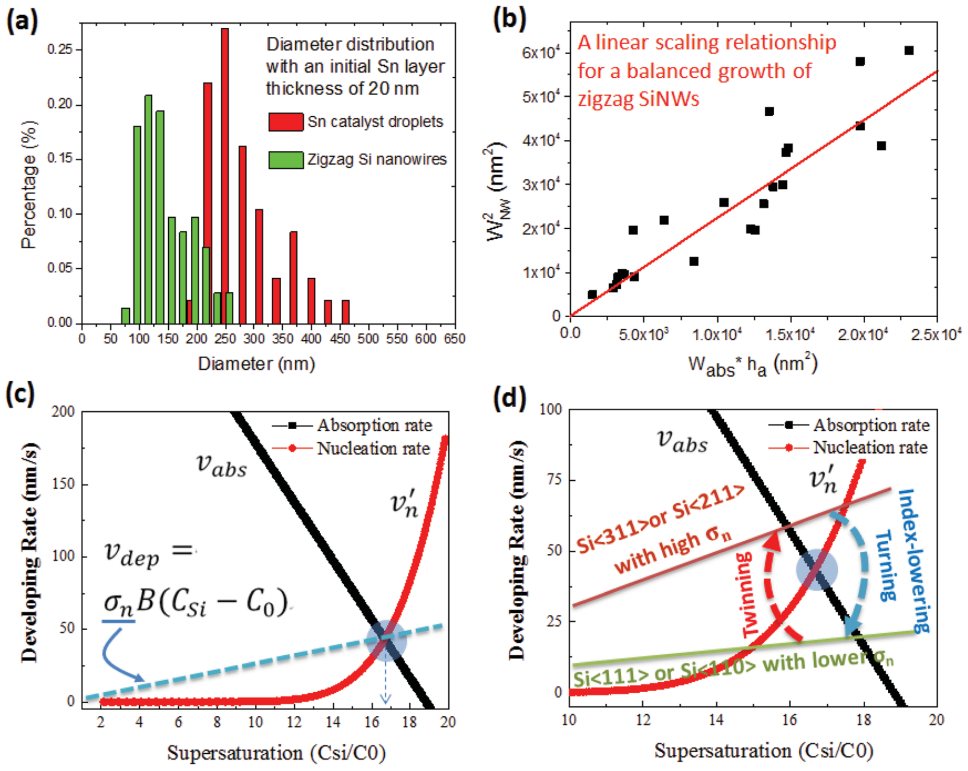


**Figure 5.** (a) shows the size-distribution histograms of the Sn catalyst droplets and the zigzag SiNWs; (b) shows a statistic plot of the deposition cross-section ($\approx W^2_{nw}$) to the absorption cross-section ($\approx W_{abs}h_a$); (c) shows the crossing point joint by the absorption rate $v_{abs}$ line and the nucleation rate $v_n'$ curve, where the deposition line of $v_{dep} = \sigma_n B(C_{Si} - C_0)$ is also supposed to go through for a balanced growth; (d) illustrates how a regular growth orientation switching, among the high-index orientations (red, with higher $\sigma_n$) and the low-index orientations (green, with lower $\sigma_n$), could help in achieving a virtual alignment and dynamics balance.

a monolayer over the deposition interface (measures $W_{nw}$ wide and $H_{nw}$ high), at an annihilation rate of

$$R_{ann} = N_n R_{in} \frac{a^2}{H_{nw} W_{nw}} = \sigma_n B(C_{Si} - C_0) \quad (2)$$

where $N_n$ is the number of co-existing nuclei sites and $\sigma_n \equiv \frac{N_n}{\frac{W_{nw} H_{nw}}{a^2}}$ is the areal density of nucleation sites at the deposition interface. In the meantime, the completion of an atomic layer adds an atomic height in the axial growth, which corresponds thus to an axial growth rate of $v_{dep} \equiv aR_{ann} = a\sigma_n B(C_{Si} - C_0)$. Thus, the temporal evolution of the number of nuclei on the deposition interface is written as

$$\frac{dN_n}{dt} = f_0 e^{-\frac{\pi k^2}{Ln(C_{Si}/C_0)}} - \frac{N_n a^2}{W_{nw} H_{nw}} B(C_{Si} - C_0) = \frac{v_n - v_{dep}}{a} \quad (3)$$

with $v_n \equiv a f_0 e^{-\frac{\pi K^2}{Ln(C_{Si}/C_0)}}$ defined as "a rate of nucleation" at the TFL edge sites/lines. In parallel, the temporal evolution of the dissolved Si atom concentration $C_{Si}$ is governed by two competing factors, the absorption flux of Si at the front a-Si:H/Sn interface and the deposition of Si atoms at the rear Sn/SiNW interface, which can be formulated as

$$\frac{dC_{Si}}{dt} * \frac{V_c}{2} = h_a W_{abs} \cdot g_{diff} \frac{D_s (C_{aSi} - C_{Si})}{L_c} - N_n B(C_{Si} - C_0) \quad (4)$$

where the first term on the right-hand side is the diffusion transport of the absorbed Si atoms from the a-Si:H/Sn interface (with a higher equilibrium Si concentration $C_{aSi}$) toward the rear deposition Sn/c-SiNW interface (with a relatively lower Si concentration $C_{Si}$), with $D_s \approx 5 \times 10^{-9} m^2\ s^{-1}$ being the diffusion coefficient of Si atoms in liquid Sn catalyst droplet and $g_{diff}$ is a geometric factor accounting for the asymmetric width for the front and the rear interface. Actually, this term also determines how fast the front a-Si:H/Sn absorption interface can pull the catalyst droplet ahead, with a velocity defined as $v_{abs} \equiv a^3 g_{diff} D_s (C_{aSi} - C_{Si})/L_c$.

Seeking a steady-state solution, over a long period of time, for the coupled rate equations of Equations (3) and (4)) with $\frac{dN_n}{dt} = \frac{dC_{Si}}{dt} = 0$, we should have $\beta v_n = v_{abs}$, where $\beta \equiv \alpha H_{nw}/h_a$ is the ratio of the SiNW height $H_{nw}$ over the a-Si:H layer thickness $h_a$. Taken the typical dimensions, we plot the modified nucleation velocity $v_n' = \beta v_n$ and the absorption velocity $v_{abs}$ together in Figure 5c, against the Si supersaturation defined as $S \equiv C_{Si}/C_0$. As we can see, $v_n'$ is a nonlinear but monotonic increasing function of $S$, which intercepts the linearly decreasing $v_{abs}$ at a balance point of $C_{Si}^* = 16.3C_0 \approx 85\%C_{aSi}$, providing a reasonable

guess of $C_{Si}$, on average and over time, at close proximity to the Sn/SiNW interface during the growth. In addition, it is also important to note that a supersaturation $S > 16$ can be established in the Sn catalyst, due to a very low equilibrium solubility of Si in Sn[31–33] and a high density supply of Si atoms from the "solid" a-Si:H thin film precursor. This value of $S > 16$ is indeed much higher than that achievable within gold, aluminum, or silver catalyst (usually with a much lower supersaturation $S \approx 1.1$ to 2, due to a high eutectic Si concentration ranging from 11% to 19%[33]). In strong contrast, during a Sn-catalyzed in-plane SiNW growth, a high number of nuclei could be rapidly created and co-exist (that is $N_n \gg 1$) at the deposition interface.

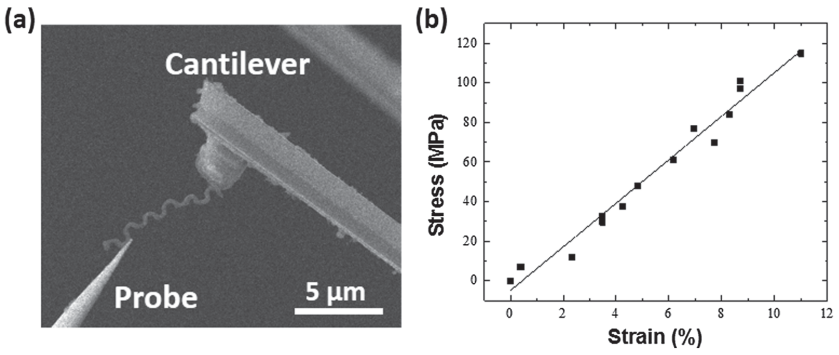


**Figure 6.** Stress–strain testing of the zigzag SiNWs spring: (a) shows SEM image of in situ stress–strain testing setup with of a segment of zigzag SiNWs mounted on the tip of a nanoprobe and to the end of a cantilever, while (b) shows the linear elastic response.

According to Equation (3), the deposition rate of $\nu_{dep} = a\sigma_n B(C_{Si} - C_0)$ is a linear function of $C_{Si}$ (thus $S$) which tends to go through the crossing point between $\nu'_n$ and $\nu_{abs}$. To achieve that, the density of nucleation sites $\sigma_n$ at the deposition interface is the only parameter to adjust the slope of $\nu_{dep}$. In a picture of the Terrace-Step-Kink (TSK) model, $\sigma_n$ can be taken as a measure of the orientation deviation of the deposition interface from the "terrace" face orientation (in c-Si, it is the most stable Si(111) facet). From an analytic and qualitative point of view, when a SiNW grows along high-index directions like Si<311> or Si<211>, the nuclei density of $\sigma_n$ is high, leading to a larger slope of $\nu_{dep}$ in Figure 5d. In contrast, when the SiNW turns into a growth direction of Si<110> or even Si<111>, the nucleation site density $\sigma_n$ becomes lower, causing a lower-lying deposition line of $\nu_{dep}$ as marked by the yellow and green lines in Figure 5d. In short, within a single domain, the continuous turning of SiNW follows an index-lowering sequence, followed by twinning behavior that reverses the sequence back into a high-index direction of Si<311> but in another twin-reflected domain. It is by this periodic turning-twinning cycling, that the system could find a "virtual" alignment of $\nu_{dep}$ that will go through the targeted crossing-point between $\nu_{abs}$ and $\nu'_n$. This explains why a regular orientation switching and zigzag SiNWs growth will be triggered automatically without any external parameter adjustment.

As for the precise self-twinning behavior at the middle of turning arms, we found that, according to Equation (1), the nuclei generation rate should increase monotonically with the local Si concentration. When the Sn catalyst droplet turns continuously, as seen in the SEM images in Figure 3c,d, the sideline in turning direction is always shorter than that of the opposite side. This indicates a shorter diffusion distance (for instance, $L_c^l < L_c^r$ in Figure 4b) and thus, according to Equation (4), a higher local Si concentration at the left TFL $C_{Si}^l > C_{Si}^r$ and a faster nucleation rate $R_n^l > R_n^r$. As the formation of a twin plane is mostly determined by the initial nucleation stacking at the TFL sites, we "speculate" that when the nuclei formation events are dominated by one specific TFL site, a coherent stacking sequence can be easily maintained. However, when the turning direction is changed or reversed, the sideline lengths are basically the same as seen in Figure 4d, with equal chances for nuclei formation on both TFL sides. This will increase the probability for a fault in stacking sequence, particularly during such a low temperature growth <350 °C. It is interesting to note that, even if multiple twinning events have been identified at the transition zone (see Figure 4f), the total number of local twin planes has to be an odd number, so as to accomplish a "reflected" switching of the growth orientation and a progressing zigzag SiNW growth. While further investigation is needed to shed more light upon the detailed twinning kinetics, our results provide the first experimental evidence that the nuclei formation at TFL sites has a "decisive" influence on the twinning and lattice quality of the as-grown SiNWs. This aspect could also indicate a new control strategy for SiNWs morphology engineering.

Finally, we come to analyze the mechanical properties of these 2D SiNW springs. A single SiNW has been picked up, as seen in the SEM image in **Figure 6**a, by using a nanomanipulator in an SEM system, and mounted between an AFM cantilever and a probe tip.[34,35] Then, the zigzag SiNW was subject to tensile strain up to 12% with the linear stress–strain response displayed in Figure 6b. This kind of testing has been repeated several times until a rupture happens at a turning corner of the zigzag SiNW. It is remarkable that this large stretchability ≈12% has been recorded with a very large SiNW of around 200 nm in diameter, which is normally supposed to break easily under stretching <1%,[4] thus an order of magnitude enhancement has been achieved with a successful 2D spring geometry engineering. In view of practical device applications, a thicker SiNW channel is also more robust and even advantageous to carry a higher current to drive the subsequent fan-out circuits. All these results thus pave the way for the development of a new generation of high performance stretchable electronics, all based on a simple low-cost and low-temperature self-assembly growth that is compatible with the mature large area thin-film technology.

## 3. Conclusions

In conclusion, we have discovered a new cyclic orientation-index-lowering turning and twin dynamics that provides large stretchability to mono-like 2D SiNW springs. Direct in situ SEM observations and HR-TEM characterizations reveal a

unique interlaced coherent domain structure bounded by precise twin-planes, which has never been documented in the literature. A growth kinetics model has been proposed to explain the regular turning-twin dynamics as a result of seeking a growth balance that requires a periodic orientation switching among major crystallographic Si orientations. We demonstrate also large elastic "stress–strain" response of the 2D SiNW springs, with a stretchability of ≈12% under tensile strain. All these results provide a whole new strategy for a rational fabrication of high-performance 2D SiNW springs, as a promising building block for all Si-based stretchable electronics.

## 4. Experimental Section

*Synthesis and Fabrication*: The fabrication procedure of the in-plane SiNWs has been illustrated schematically in Figure 1a–c, which involve respectively (1) first, the evaporation of Sn pads of ≈40 nm thick and 10 μm × 10 μm wide on glass substrate, in a plasma-enhanced chemical vapor deposition (PECVD) system; (2) then, a $H_2$ plasma treatment at 280 °C for 5 min, during which the Sn pads were transformed into separate Sn droplets of 200–600 nm in diameter, see also the SEM (Zeiss Sigma) image in Figure 1d for details; (3) a deposition of 30 nm hydrogenated amorphous Si (a-Si:H) thin film at lower $T_{sub} = 120$ °C such that the Sn droplets remain solid; (4) finally, when the substrate temperature was raised to 340 °C, the Sn droplets melt again and start to take in nearby a-Si:H layer to produce crystalline SiNWs along their moving courses.

*In Situ SEM Observation*: For in situ SEM observation, the samples after a-Si:H coating were unloaded from the PECVD chamber and mounted onto a heating stage in a Zeiss Sigma SEM system. The in-plane SiNWs growth can be activated without any gaseous supply that would otherwise degrade the high vacuum environment in SEM observation. Typically, the SiNW was activated to grow at 340 °C, upon a heating stage within SEM chamber in a vacuum of $<5 \times 10^{-5}$ Pa.

*In Situ Mechanical Testing*: The zigzag SiNW was handled by using a nanomanipulator (Kleindiek MM3A) in an SEM system, being mounted at one end to an AFM cantilever (Veeco CLFC-NOBO) and the other to the probe tip, as seen in the SEM image shown in Figure 6a. Details of the technical aspects in SiNW fixing and operations are available elsewhere (see refs. [34] and [35] in the text).

## Supporting Information

Supporting Information is available from the Wiley Online Library or from the author.

## Acknowledgements

The authors acknowledge the financial support from National Basic Research 973 Program under Grant Nos. 2014CB921101, MOST: 2012CB932702, and NSFC under Grant Nos. 61321001, 11274155, and 61204050, Jiangsu Province Natural Science Foundation (Young Talent Program No. BK20130573), Scientific and Technological Support Programme in Jiangsu province under Grant No. BE2014147-2, and Jiangsu Shuangchuang Team's and Personal Program and the Fundamental Research Funds for the Central Universities.

Received: February 13, 2016
Revised: March 27, 2016
Published online: May 24, 2016

[1] L. Wang, P. Liu, P. Guan, M. Yang, J. Sun, Y. Cheng, A. Hirata, Z. Zhang, E. Ma, M. Chen, X. Han, *Nat. Commun.* **2013**, *4*, 2411.
[2] L. Wang, K. Zheng, Z. Zhang, X. Han, *Nano Lett.* **2011**, *11*, 2382.
[3] K. Zheng, X. Han, L. Wang, Y. Zhang, Y. Yue, Y. Qin, X. Zhang, Z. Zhang, *Nano Lett.* **2009**, *9*, 2471.
[4] Y. Zhu, F. Xu, Q. Qin, W. Y. Fung, W. Lu, *Nano Lett.* **2009**, *9*, 3934.
[5] D.-Y. Khang, H. Jiang, Y. Huang, J. A. Rogers, *Science* **2006**, *311*, 208.
[6] H. W. Kim, S. H. Shim, *Appl. Surf. Sci.* **2007**, *253*, 3664.
[7] H. F. Zhang, C. M. Wang, E. C. Buck, L. S. Wang, *Nano Lett.* **2003**, *3*, 577.
[8] F. Xu, W. Lu, Y. Zhu, *ACS Nano* **2011**, *5*, 672.
[9] S. Y. Ryu, J. Xiao, W. I. Park, K. S. Son, Y. Y. Huang, U. Paik, J. A. Rogers, *Nano Lett.* **2009**, *9*, 3214.
[10] J. W. Durham, Y. Zhu, *ACS Appl. Mater. Interfaces* **2013**, *5*, 256.
[11] S.-W. Hwang, C. H. Lee, H. Cheng, J.-W. Jeong, S.-K. Kang, J.-H. Kim, J. Shin, J. Yang, Z. Liu, G. A. Ameer, Y. Huang, J. A. Rogers, *Nano Lett.* **2015**, *15*, 2801.
[12] J. Kim, M. Lee, H. J. Shim, R. Ghaffari, H. R. Cho, D. Son, Y. H. Jung, M. Soh, C. Choi, S. Jung, K. Chu, D. Jeon, S.-T. Lee, J. H. Kim, S. H. Choi, T. Hyeon, D.-H. Kim, *Nat. Commun.* **2014**, *5*, 5747.
[13] A. Chortos, Z. Bao, *Mater. Today* **2014**, *17*, 321.
[14] B. Tian, P. Xie, T. J. Kempa, D. C. Bell, C. M. Lieber, *Nat. Nano* **2009**, *4*, 824.
[15] A. Lugstein, M. Steinmair, Y. J. Hyun, G. Hauer, P. Pongratz, E. Bertagnolli, *Nano Lett.* **2008**, *8*, 2310.
[16] I. R. Musin, M. A. Filler, *Nano Lett.* **2012**, *12*, 3363.
[17] A. Pevzner, Y. Engel, R. Elnathan, A. Tsukernik, Z. Barkay, F. Patolsky, *Nano Lett.* **2012**, *12*, 7.
[18] R. E. Algra, M. A. Verheijen, M. T. Borgström, F. Lou-Fé, I. George, W. J. P. Van Enckevort, V. Elias, E. P. A. M. Bakkers, *Nature* **2008**, *456*, 369.
[19] N. Shin, M. Chi, J. Y. Howe, M. A. Filler, *Nano Lett.* **2013**, *13*, 1928.
[20] L. Yu, P.-J. Alet, G. Picardi, P. Roca i Cabarrocas, *Phys. Rev. Lett.* **2009**, *102*, 125501.
[21] L. Yu, W. Chen, B. O'Donnell, G. Patriarche, S. Bouchoule, P. Pareige, R. Rogel, A. C. Salaun, L. Pichon, P. Roca i Cabarrocas, *Appl. Phys. Lett.* **2011**, *99*, 203104.
[22] L. Yu, M. Xu, J. Xu, Z. Xue, Z. Fan, G. Picardi, F. Fortuna, J. Wang, j. xu, Y. Shi, K. Chen, P. Roca i Cabarrocas, *Nano Lett.* **2014**, *14*, 6469.
[23] I. Scarontich, R. Car, M. Parrinello, *Phys. Rev. B* **1991**, *44*, 11092.
[24] S. Roorda, S. Doorn, W. C. Sinke, P. M. L. O. Scholte, E. van Loenen, *Phys. Rev. Lett.* **1989**, *62*, 1880.
[25] K.-K. Lew, J. M. Redwing, *J. Cryst. Growth* **2003**, *254*, 14.
[26] H. Jeong, T. E. Park, H. K. Seong, M. Kim, U. Kim, H. J. Choi, *Chem. Phys. Lett.* **2009**, *467*, 331.
[27] F. Glas, J.-C. Harmand, G. Patriarche, *Phys. Rev. Lett.* **2007**, *99*, 146101.
[28] C. Y. Wen, J. Tersoff, M. C. Reuter, E. A. Stach, F. M. Ross, *Phys. Rev. Lett.* **2010**, *105*, 195502.
[29] C. Jayaprakash, C. Rottman, W. F. Saam, *Phys. Rev. B* **1984**, *30*, 6549.
[30] E. E. Gruber, W. W. Mullins, *J. Phys. Chem. Solids* **1967**, *28*, 875.
[31] J. Kühnle, R. B. Bergmann, J. H. Werner, *J. Cryst. Growth* **1997**, *173*, 62.
[32] C. D. Thurmond, *J. Phys. Chem.* **1953**, *57*, 827.
[33] V. Schmidt, J. V. Wittemann, U. Gösele, *Chem. Rev.* **2010**, *110*, 361.
[34] X. Li, X. Wei, T. Xu, D. Pan, J. Zhao, Q. Chen, *Adv. Mater.* **2015**, *27*, 2852.
[35] X. Li, X. L. Wei, T. T. Xu, Z. Y. Ning, J. P. Shu, X. Y. Wang, D. Pan, J. H. Zhao, T. Yang, Q. Chen, *Appl. Phys. Lett.* **2014**, *104*, 103110.